# Oligomerization of the antimalarial drug target *Pf*ATP4 is essential for parasite survival

Aarti A. Ramanathan[*], Joanne M. Morrisey[*], Thomas M. Daly[*], Lawrence W. Bergman[*], Michael W. Mather[*], Akhil B. Vaidya[*†]

[*]Drexel University College of Medicine, Philadelphia, PA 19129

[†]To whom correspondence may be addressed

Email: av27@drexel.edu, Tel: +1-215.991.8557



**Classification**
Biochemistry, Microbiology
**Keywords**
PfATP4, Antimalarial drug target, Plasmodium falciparum, P-Type ATPase

## Abstract

*Plasmodium falciparum* P-type ATPase (*Pf*ATP4) is a $Na^+$ efflux pump crucial for maintaining low $[Na^+]_i$ in malaria parasites during their intraerythrocytic development cycle. In recent years, multiple studies have shown *Pf*ATP4 to be the target of a large number of chemical scaffolds, including current candidate antimalarials KAE609 and SJ733. Here we show that *Pf*ATP4 exists as a large complex. Immunopurification and proteomic studies revealed the complex to be homooligomeric in nature. The complex appears to be assembled co-translationally. Phylogenetic analysis suggests that ATP4 from apicomplexans and chromerids form a distinct class of P-type ATPases having fewer transmembrane helices compared to their orthologues. We hypothesized that reduction of transmembrane helices in *Pf*ATP4 might necessitate oligomerization to maintain its function. We further suspected potential involvement of π-π interactions between aromatic amino acids within the terminal transmembrane helix of each monomer to be critical for oligomerization. To test this hypothesis, we mutated three aromatic amino acids in the last transmembrane helix of *Pf*ATP4. Wildtype and the mutated *Pf*ATP4 genes were introduced at an ectopic locus in a *P. falciparum* line, in which endogenous *Pf*ATP4 was conditionally expressed. Whereas the wildtype copy of *Pf*ATP4 expressed from the ectopic locus was able to form the oligomeric complex, the mutant *Pf*ATP4 failed to do so. Strikingly, unlike the wildtype, the mutant *Pf*ATP4 failed to functionally complement the knockdown of the endogenous gene, leading to parasite demise. These results strongly suggest that co-translational oligomerization of *Pf*ATP4 is essential for its function and for parasite survival.




## Significance Statement

*Plasmodium falciparum* ATP4 (*Pf*ATP4) is a $Na^+$ efflux pump and is the target of at least two antimalarial drug candidates (KAE609, SJ733) currently in clinical trials. With a rapid parasite clearance rate ($t_{99}$=12h) in initial clinical studies, *Pf*ATP4-active drugs present the prospect of taking us a step closer to

malaria elimination in a world that is currently threatened by artemisinin resistance. In this study, we have established that *Pf*ATP4 exists as a homo-oligomeric complex, which is assembled co-translationally through interactions facilitated by aromatic amino acids in its last transmembrane helix. Crucially, its existence as a complex is essential for its function. This exposes a vulnerability in the target that could be potentially exploited for drug design.

## Main text

### Introduction

In response to the constant threat of emerging resistance to existing antimalarials, significant efforts have been undertaken for discovery and development of new antimalarials. From millions of compounds subjected to high-throughput screening, more than 30,000 compounds were found to have the ability to inhibit *Plasmodium falciparum* growth *in vitro (*1-3*).* In spite of this large number of compounds with antimalarial activity, there are only a limited number of targets that have been identified. Over the last decade, several clinical candidates have emerged for further development (4). Among these are KAE609, SJ733 and PA21A092 that target the *P. falciparum* $Na^+/H^+$ pump named *Pf*ATP4 (5-8). Inhibition of *Pf*ATP4 results in an increased $[Na^+]$ inside the parasite cytoplasm (9). As a consequence, multiple events such as swelling of the parasite (8, 10), changes in the lipid composition of the parasite plasma membrane (PPM) and premature schizogony (11), and eryptosis (7) seem to contribute to parasite demise. Interestingly, 7-9% of the collection of antimalarial compounds included in the Malaria and the Pathogen Boxes distributed by Medicines for Malaria Venture (MMV) appear to inhibit *Pf*ATP4 as judged by their ability to cause $Na^+$ influx into the parasite and disruption of lipid homeostasis within the PPM (12-14). Resistance to several of these compounds has been shown to be associated with mutations in *Pf*ATP4 (5, 7, 8, 15, 16). If one were to extrapolate the proportion of *Pf*ATP4 inhibitors found in the Malaria and Pathogen Boxes to all the antimalarial compounds identified by the high-throughput screening campaigns, one would predict that thousands of potential

antimalarials target *Pf*ATP4, making it a highly druggable target in the malaria parasite.

*Pf*ATP4 belongs to a superfamily of P-type molecular machines that use phosphorylation-dephosphorylation cycles and ATP hydrolysis to transport ions across membranes (17). These pumps are divided into 5 classes (PI to PIV), which are further divided into subclasses (A, B, C etc.) based on their function and membrane localization (18, 19). *Pf*ATP4 belongs to the PII class, of which sarco/endoplasmic reticulum $Ca^{2+}$ ATPase (SERCA) and $Na^{+}/K^{+}$ ATPase have been extensively investigated at the structure-function level (20-26). Despite low sequence similarity, all P-type ATPases share common structural features, with large cytoplasmic domains connected to several transmembrane helices, accompanied by an additional regulatory domain in some cases. As first revealed by the high resolution structure of SERCA, the cytoplasmic portion is divided into 3 domains: phosphorylation (P), nucleotide binding (N) and actuator (A) domains, while the integral membrane portion, consisting of multiple transmembrane helices, is divided into two domains: transport domain (T) involved in ion transport, and the support domain (S) (27). Multiple X-ray crystal structures of intermediate states of the catalytic cycle of SERCA have revealed massive structural rearrangements of the cytoplasmic and the T domains. During this cycle, the S domain remains relatively immobile and is believed to provide structural stability to support appropriate functioning of the pump.

*Pf*ATP4 is currently categorized as a member of the PIID subfamily of pumps. Pumps belonging to this family are limited to fungi, lower plants and some unicellular eukaryotes, and function to transport monovalent alkali cations (28, 29). There is no structural information available at present for this subfamily. Sequence-based transmembrane helix predictions project 8 membrane helices in apicomplexan and chromerid ATPases rather than the 10-11 found in the ATPases from the rest of the PIID family members (*SI Appendix, Additional data 1*). At this point, we do not know how this alteration of the transmembrane domains affects the functioning of this protein. Given that *Pf*ATP4 is an attractive drug target belonging to this subgroup, we sought to characterize it further. We

provide evidence that, unlike other characterized PII ATPases that function in their monomeric form, *Pf*ATP4 requires oligomerization and interfering with this process results in parasite demise likely due to compromised catalytic function of the protein.

## Results

### *Phylogenetic comparison of PfATP4 within PIID type ATPases*

Phylogenetic analysis was carried out after aligning the *Pf*ATP4 amino acid sequence with representative PIID type ATPases and with select members of PIIA (SERCA) as an outgroup. PIID ATPases fell into two distinct groups, one comprising of pumps from fungi, kinetoplastids, bryophytes and Entameoba and the other consisting of chromerid, apicomplexan, stramenophile, chlorophyte and dinoflagellate pumps. Among the latter, apicomplexan and chromerid PIID ATPases branch together with strong support (*Fig. 1a and SI Appendix, Fig. S1*). The general domain configuration of PII type ATPase is shown in *SI Appendix, Fig. S2a*. The order of the cytoplasmic and the transmembrane domains of PII type ATPases is such that the actuator and phosphorylation domains are formed by two different segments of the protein, each separated by either the transport domain helices T1 and T2 (for A domain) or by the N domain (for P domain). This is followed by T5, T6 and the S domains consisting of S1-S4/S5 transmembrane helices. Thus, most PII type ATPases contain 10-11 transmembrane helices (T1-T6, S1-S4 or S5). In some cases, these are additionally accompanied by a regulatory subunit (25, 26, 30). The transmembrane domain predictions of chromerid and apicomplexan PIID ATPases, however, revealed membrane domains apparently consisting of only 8 transmembrane helices (*SI Appendix, Additional data 1*). This unique feature of apicomplexan and chromerid PIID ATPases suggests the possibility that these pumps might be divergent in structure and in some details of their mode of operation compared to other PII ATPases.

### *PfATP4 is present as a large complex in the blood stage of the malaria parasite*

In order to study *Pf*ATP4, we generated transgenic parasites expressing endogenous *Pf*ATP4 tagged with a c-Myc epitope at the C terminal end under the control of the TetR:DOZi aptamer system using single crossover recombination in NF54*attB* parasite line ( called NF54*attB:PfATP4Myc; SI Appendix, Fig. S3a*). With this conditional expression system, expression of the target protein is maintained during growth in the presence of anhydrotetracycline (aTc). After successful integration, knockdown of *Pf*ATP4 by the removal of anhydrotetracyline (aTc) was confirmed by using both anti-c-Myc and anti-*Pf*ATP4 antibodies (*SI Appendix, Fig. S3b*). As observed in a previous study (31), *Pf*ATP4 knockdown caused parasite demise (*SI Appendix, Fig. S3c*). Western blot analysis of membrane preparations from these parasites revealed the presence of *Pf*ATP4 as a 140 kDa protein in SDS-polyacrylamide gel electrophoresis (PAGE; *Fig.1b*). When the same samples were subjected to blue native (BN)-PAGE, the protein migrated as a higher molecular weight complex (*Fig.1c*). This complex was not disrupted upon treatment with reducing agents, increased salt concentration, sonication, or freeze thawing (*Fig.1d*). To ensure that the band observed was not an artifact of BN-PAGE conditions, we combined digitonin solubilization of samples with additional ionic detergents or a chaotropic agent. Inclusion of SDS below its critical micellar concentration (CMC) did not disrupt the complex. However, treatment with deoxycholate below its CMC, or with 8M urea disrupted the complex (*Fig.1d and SI Appendix, Fig. S4a*). Although we did not detect monomeric *Pf*ATP4 in BN-PAGE when the complex was disrupted, the same samples when subjected to SDS-PAGE revealed the monomeric form (*SI Appendix, Fig. S4a, bottom panel and S4b*). In the SDS-PAGE analysis of urea-treated samples, we noticed higher molecular weight aggregates of *Pf*ATP4 suggesting that our inability to observe the monomeric form in BN-PAGE likely resulted from aggregation of the highly hydrophobic protein.

### *PfATP4 exists as a homooligomeric complex*

The presence of *Pf*ATP4 as a higher molecular weight complex could be a result of its association with other proteins, or from its existence as a homooligomer *in-situ.* To distinguish between these possibilities we carried out non-denaturing immunopurification from *NF54attB*:*Pf*ATP4*Myc* tagged line using anti-c-Myc coated beads. Untagged *NF54attB* parasites were used as a control. Immunopurification of *Pf*ATP4 maintained it as a multimeric complex (*Fig. 2a and Fig. 2b*). Immunopurified samples from the untagged and the tagged parasites were examined by proteomic analysis involving trypsin digestion followed by LC-MS/MS. This analysis was carried with two biological replicates. Whereas no peptide spectra originating from *Pf*ATP4 were seen in control samples, greater than 50% of the total *P. falciparum*-specific spectra from the tagged samples originated from *Pf*ATP4 covering >95% of the protein (*Fig. 2c and SI Appendix, Additional dataset S2*). No other *P. falciparum*-specific proteins were represented uniquely at a significant level in the tagged samples. The absence of any other parasite encoded proteins in the complex, therefore, supports the proposition that the large complex is formed by homooligomerization of *Pf*ATP4. At present we are unable to determine the stoichiometry of the oligomer.



### *PfATP4 complex is assembled co-translationally*

To investigate the process of *Pf*ATP4 complex assembly, we generated a merodiploid parasite line in which a copy of constitutively expressed *Pf*ATP4 (originating from the *Dd2* strain and tagged with a 3xHA epitope) was integrated at the *cg6::attB* locus (32), in addition to the c-Myc tagged endogenous *Pf*ATP4 locus (*NF54* strain) that was conditionally regulated by the TetR:DOZi system (*Fig. 3a, 3b and SI Appendix, Fig. S5a*). Conditional knockdown of the endogenous *Pf*ATP4 expression by withdrawing aTc, which otherwise resulted in parasite demise (*SI Appendix, Fig. S3c*), was complemented by the presence of ectopically expressed *Pf*ATP4 (*Fig. 4d*). Both the copies of *Pf*ATP4 were co-dominantly expressed in the merodiploid parasite line and formed distinct oligomeric complexes (*Fig. 3c and 3d*). To gain an understanding of the

assembly process, we considered that co-translational assembly would lead to non-hybrid complex formation, because proximity of the monomers would be crucial for this process, whereas the formation of hybrid or mixed complexes would indicate that the assembly process was likely post-translational. To test if *Pf*ATP4 formed hybrid or non-hybrid complexes, digitonin solubilized parasite material was subjected to immunopulldown with either anti-c-Myc or anti-HA antibodies from the merodiploid parasites. The eluates were examined by SDS-PAGE followed by Western blots probed with either anti-c-Myc or anti-HA antibodies. If *Pf*ATP4 formed hybrid complexes, cross-probing after immunopulldown should result in a positive band. The absence of a positive band after cross-probing suggested that *Pf*ATP4 did not form hybrid complexes: pulldown of *Pf*ATP4:Myc reacted with anti-c-Myc but not with anti-HA antibody and vice versa (*Fig. 3e*) . This was further supported by utilizing the fact that a single polymorphism at position 1128 distinguishes *Pf*ATP4 of the NF54 strain from its counterpart in Dd2 (G1128 in NF54 and R1128 in Dd2). Proteomic analysis of eluates by LC-MS/MS revealed the presence of G1128 spanning peptides *only* in c-Myc eluted samples and R1128 spanning peptides predominantly in HA eluted samples (*Fig. 3f and SI Appendix, Additional Dataset S2*). We interpret these results to show that homooligomeric *Pf*ATP4 complexes are formed co-translationally.



***Transmembrane helix TM8 plays a critical role in oligomerization of PfATP4***

Extensive structural analysis of SERCA in different E1-E2 states has shown that ion transport in P type ATPase is accompanied by significant structural rearrangements in both the cytoplasmic and the T domains. The structural stability and support for these movements appears to be provided by the relatively immobile S domain (33). We hypothesized that the reduced number of transmembrane helices in *Pf*ATP4 may compromise its ability to function as a monomer, thereby necessitating oligomerization to provide the stability to support the dynamic movements that accompany ion transport. Close examination of the last transmembrane helix of *Pf*ATP4 (TM8) revealed the presence of multiple

bulky aromatic amino acids (*Fig. 4b*). Helical wheel projections of the sequence indicated that the aromatic residues W1231, F1238 and F1245 likely reside on the same face of the TM8 helix, suggesting the possibility that these aromatic amino acids might participate in inter-monomer π-π stacking favoring oligomerization of the pump.

To test this hypothesis we carried out mutagenesis of the three aromatic amino acids (W1231A, F1238V, F1245V). The mutated *Pf*ATP4 allele (*Pf*ATP4:TM8Mut) was tagged with a 3xHA epitope and introduced at the *cg6::*attB locus into the parasite line carrying endogenous *Pf*ATP4 tagged with the c-Myc epitope under the control of the TetR:DOZi aptamer system (*Fig. 4a and SI Appendix, Fig. S6*). In the presence of aTc, the *Pf*ATP4 alleles from both loci were co-dominantly expressed (*Fig. 4c*). The ability of both the wild type and the mutated allele to complement endogenous *Pf*ATP4 knockdown was tested by the withdrawal of aTc from the medium. While the wildtype allele could functionally complement the *Pf*ATP4 deficiency, the mutated allele failed to do so (*Fig. 4d*). BN-PAGE analysis of the protein from both merodiploid lines showed that whereas *Pf*ATP4 arising from the wildtype allele at the ectopic locus formed an oligomeric complex, no complex formation was observed from the mutated *Pf*ATP4 allele (*Fig. 4e*). These results strongly suggest that *Pf*ATP4 complex formation involves the aromatic amino acids in the TM8 helix, and that this is critical for the survival of the parasite.



## Discussion

Maintenance of intracellular ion homeostasis is a pre-requisite for life. All organisms maintain low [$Na^+$] in their cytoplasm and often expend enormous amount of energy for this purpose. Intraerythrocytic malaria parasites are initially exposed to the low [$Na^+$] of the host cell cytoplasm. However, as the parasite progresses through its developmental cycle, the [$Na^+$] gradually increases in the host cell cytoplasm due to new channels exported from the parasite and inserted into the erythrocyte plasma membrane, eventually exposing the parasites to

[$Na^+$] levels equal to that in the extracellular environment (34). To sustain their normal physiological processes, parasites need to extrude $Na^+$ from their cytoplasm, a process proposed to be mediated by *Pf*ATP4. Thus, inhibition of *Pf*ATP4 causes disruption of ion homeostasis, resulting in parasite death. In the last decade, *Pf*ATP4 activity has been found to be inhibited by a large number of chemical scaffolds, indicating that it is a highly druggable target. It is reasonable to assume that the structural features of *Pf*ATP4 underlie its promiscuity as an antimalarial drug target. Here, we describe initial investigations of *Pf*ATP4 structure in its native state. Our data suggest *Pf*ATP4 to exist as a homooligomeric complex and this oligomerization is essential for parasite survival.

The movement of ions across lipid bilayers by P-type ATPases is a multi-step process and is described by the Post-Albers cycle (18, 25, 33, 35, 36). The pump acts both as a kinase and a phosphatase, as well as a conduit for its substrate. The catalytic cycle is accompanied by massive conformational changes within the cytosolic domains of the pump and vertical movements of the transmembrane helices of the T domain, whereas the S domain helices remain relatively unchanged. The transmembrane bundle formed by the S domain has been suggested to serve as an anchor within the membrane providing the stability needed for the catalytic cycle (33, 37-39). Most type PII ATPases have at least 4 such helices to serve this purpose. The fact that apicomplexan and chromerid PIID ATPases contain fewer transmembrane helices may result in their reduced ability to provide the needed stability for the catalytic function of the pump. We suggest that *Pf*ATP4 can only function as a homooligomeric complex and that this is essential to compensate for the reduced stability of the monomer during the catalytic cycle. We have provided evidence suggesting that the homooligomeric structure of *PfATP4* involves the aromatic amino acids in the last transmembrane helix (TM8) of the protein. These data are consistent with the interpretation that interactions between the aromatic amino acids within this region are critical not just for complex formation but also for enzymatic function of the protein and maintenance of ion homeostasis within the parasite. It is

interesting to note that a recent structural study (40) on plasma membrane type PIIB $Ca^{2+}$ ATPase (PMCA) revealed π-π interactions between aromatic amino acids within the last transmembrane helix of the pump and those in its obligatory subunit basigin (or neuroplastin). Thus, such interactions with functional significance have precedence in other P-type ATPases.

Our results also show that homooligomerization of *Pf*ATP4 occurs co-translationally: *Pf*ATP4 expressed from two different loci do not form hybrid complexes. Co-translational assemblies of complexes have been reported in other systems (41, 42). To our knowledge, however, this is the first observed instance of co-translational assembly in a malaria parasite. The process of co-translational assembly of transmembrane proteins presents additional challenges. One could imagine the requirement of specific factors and chaperones that maybe involved for appropriate assembly of such complexes. Attempts by multiple investigators to express functional *Pf*ATP4 in heterologous systems have been challenging thus far (personal communication from Case McNamara, Kiaran Kirk and Raymond Hui). The absence of parasite specific factors in heterologous systems required for co-translational assembly could underlie the inability to express functional *Pf*ATP4. The requirement of co-translational assembly of *Pf*ATP4 for parasite survival points to a potential vulnerability that could be exploited for drug design. At this point, however, compounds such as KAE609 and PA21A092 that inhibit *Pf*ATP4 do not disrupt complex formation (data not shown), and thus are not likely to be interfering with this process. It would be of interest to investigate whether some of the other chemical scaffolds that target *Pf*ATP4 have the ability to disrupt complex formation. Although we have not determined the stoichiometry of the complex, given the π-π interactions within its TM8 helices, it may be reasonable to propose it to be dimeric in nature. Determination of the structure of the complex should provide definitive answer.



## Materials and Methods

### *P. falciparum culture*

*P. falciparum* NF54*attB* parasites were a gift from David Fidock at Columbia University. Asexual parasites were cultured in Human ($O^+$) blood (purchased from Interstate blood bank in Tennessee), at 2.5% hematocrit in RPMI1640 medium supplemented with 0.5% Albumax, 2 $gl^{-1}$ $NaHCO_3$, 15 mM HEPES-K pH 7.4 , 1 mM hypoxanthine and 50 mg $l^{-1}$ gentamicin in 90% $N_2$, 5% $O_2$ and 5% $CO_2$. Additionally, transgenic parasites were supplemented with 250 nM of aTc for routine culture, unless indicated otherwise. Periodically, mycoplasma testing was done to ensure that the cultures were mycoplasma negative.



### *Plasmid construction and generation of transgenic parasites*

To generate conditional knockdown of endogenous NF54*Pf*ATP4:Myc tagged parasites, we utilized the TetR:Dozi aptamer system. The original pMG75-ATP4 vector (**31**) was a kind gift from Jacquin Niles at MIT. To facilitate recombination at the endogenous locus, the original vector was modified to remove the *attP* site (43). Methods for generation of NF54*Pf*ATP4Myc, and merodiploid NF54*Pf*ATP4Myc*attB*:*Pf*ATP4:wt and NF54*Pf*ATP4Myc*attB*:*Pf*ATP4:TM8Mut parasite lines are described in *SI Appendix*.

### Phylogenetic analysis

Sequences of PIID ATPases from species representing a broad range of eukaryotic groups were identified from previous studies (29, 44) and BLAST (45) searches of NCBI (46) and EupathDB (47) databases. The sequences chosen for alignment are listed in *SI Appendix Table 1*. Details of software packages used for phylogenetic analysis are given in *SI Appendix Methods*.

### *Membrane preparations of NF54PfATP4:Myc tagged parasites*

Trophozoite stage parasites (~$10^{10}$) were percoll enriched and released from RBCs by treating with 0.05% Saponin + 1 µg/ml fungal protease inhibitor cocktail (Sigma–Aldrich, Inc) in lysis buffer containing 120 mM KCl, 20 mM NaCl, 20 mM glucose, 6 mM HEPES, 6 mM MOPS, 1mM $MgCl_2$ and 0.1 mM EGTA, pH 7.0,

parasites were spun down at 3000 rpm for 5 mins, at 4°C. An additional one or two washes were performed in the same buffer until hemoglobin color was undetectable. After the washes the parasite pellet was resuspended in membrane dissociation buffer containing 10 mM KCl, 10 mM Glucose, 10 mM HEPES, 1 mM EDTA, 1 mM PMSF, 250 mM Sucrose and 1 µg/ml fungal protease inhibitor cocktail. All steps were performed at 4 °C. The parasite pellet was resuspended in 10x volume of the membrane dissociation buffer and pressurized with compressed nitrogen in a 4639 cell disruption bomb ($N_2$ bomb, Parr, USA) at 1000psi. Upon completion of nitrogen cavitation another aliquot of the protease inhibitors was added. The lysed sample was centrifuged at low speed (900g) for 10 min to remove cell debris and hemozoin. Following this, the supernatant was collected and centrifuged at intermediate-speed (23,000g) for 20 min to remove intact organelles. Pellet was discarded, and supernatant was subjected through a final high-speed centrifugation step (200,000g) for 30 min to obtain the membrane pellet. Membrane pellet was resuspended in buffer containing 10 mM KCl, 10 mM HEPES, 1 mM EDTA and 250 mM sucrose and flash frozen in liquid nitrogen before storage at -80 °C.



***SDS/BN-PAGE***

For SDS-PAGE, parasite pellets were obtained by 0.05% saponin treatment of infected RBCs in the presence of 1 µg/ml protease and phosphatase inhibitors. The harvested pellet was further lysed in 5x pellet volume in buffer containing 4% SDS, 0.5% Triton-X in PBS. Protein concentration was estimated and 20-50 µg of the total protein was loaded onto each lane and electrophoresis was performed using a standard protocol. For BN-PAGE, membranes or saponin-lysed parasite pellets were solubilized overnight at 4 °C in solubilization buffer containing 200 mM 6-aminocaproic acid, 50 mM Bis-tris, pH 7, 1 mM EDTA, 1 mM AEBSF, 2 µg/ml fungal protease and phosphatase inhibitors with digitonin at indicated ratios, or at 2% unless otherwise indicated. The solubilized sample was centrifuged at 14,000 rpm for 15 min at 4 °C and supernatant was collected for BN-PAGE. NativePAGE™ Novex® Bis-Tris Gel System (Invitrogen) was used for

running BN-gels. 5% G-250 Coomassie dye was added to the solubilized sample (20-50 µg/lane) at a detergent:dye ratio of 4:1 by weight before addition of the Native-PAGE sample buffer. The sample was loaded in a NativePAGE™ 4-16% Bis-Tris gradient gel and was run on ice with pre-chilled buffers for a total of ~1.5 ± 0.2 h, the first 30 min at 150V with dark-blue cathode buffer, after which dark-blue cathode buffer was replaced with light-blue cathode buffer and the voltage was increased to 250V for the remaining time, until the dye front reached the gel bottom.

***Immunoblotting***

BN-PAGE gels were wet transferred overnight (~16 ± 2 h) at 35 V, 4 $^{o}$C onto a 0.45 µM PVDF membrane using NuPAGE transfer buffer (Invitrogen). The membrane was fixed with 8% acetic acid for 15 min, was air-dried and then washed with methanol three times for 10 mins to remove Coomassie blue dye. The native marker was pencil-marked to size on the transferred membrane after the first methanol wash. After a quick rinse with deionized water to remove methanol, the membrane was blocked with 5% skim milk for 2 h, and probed with primary antibody overnight (Rabbit Anti-Myc mAb, Clone 71D10 Cell signaling,; Mouse Anti-HA mAb, Clone F7, Santacruz, Mouse Anti-*Pf*ATP4 sera, see SI appendix, Methods), at 4 $^{o}$C. Membranes were washed with TBS, 0.02% tween and probed with appropriate secondary for at least 2 h at room temperature, and developed with SuperSignal West pico and femto substrate mixed in 9:1 ratio (Thermo scientific). SDS-PAGE gels were transferred using 25 mM Tris, 192 mM glycine and 20% methanol. Following transfer, the membrane was blocked and subsequent steps were performed as described above.

***Immunopulldown***

Parasite pellets from both wildtype and *Pf*ATP4-tagged strains were solubilized overnight in solubilization buffer containing 2% digitonin, and supernatant was harvested as described above (see methods for BN-PAGE). Antibody coated Dynabeads (Pierce Anti-HA, Clone 2-2.2.14 or Anti-c-Myc, Clone 9E10; Thermo

Fisher Scientific) were washed 3 times in 1x PBS, and 1.5 mg of solubilized total protein was bound to 100 µl of the beads, overnight on rotation at 4 °C. Protein-bound beads were washed three times with 1x PBS + 0.063% digitonin and eluted three times each with 100 µl of either HA (2 mg/ml) or c-Myc (0.75 mg/ml) peptides at room temperature, for 15 min on rotation. Eluant was pooled and concentrated to 30 µl using a 3 kDa regenerated cellulose cutoff concentrator (Millipore). Proteins were reduced with 1x Lammelli buffer and run for 0.5 cm on an SDS-PAGE gel, fixed with 40% MeOH and 10% acetic acid, stained with 0.1% Coomassie blue dye, excised and sent for LC-MS/MS analysis in 30% acetonitrile and 50 mM ammonium carbonate to the Rutgers Biological Mass Spectrometry facility.



***Proteomic analysis***

***In-gel digestion:*** Each gel band was subjected to reduction with 10 mM DTT for 30 mins at 60 °C, and alkylation with 20 mM iodoacetamide for 45 min at room temperature in the dark and overnight digestion with trypsin (Sequencing grade, Thermo Fisher Scientific) at 37 °C. Peptides were extracted twice with 5% formic acid, 60% acetonitrile and dried under vacuum.

***Liquid chromatography-tandem mass spectrometry (LC-MS/MS)****:* Samples were analyzed using a Q Exactive HF tandem mass spectrometer coupled to a Dionex Ultimate 3000 RLSCnano System (Thermo Scientific). Samples were loaded on to a fused silica trap column Acclaim PepMap-100, 75 µm x 2 cm (Thermo Scientific). After washing for 5 min at 5 µl/min with 0.1% trifluoroacetic acid, the trap column was brought in-line with an analytical column (Nanoease MZ peptide BEH C18, 130 Å, 1.7 µm x 75 µm x 250 mm, Waters) for LC-MS/MS. Peptides were eluted using a segmented linear gradient of 4 to 90% B (A: 0.2% formic acid, B: 0.08% formic acid, 80% acetonitrile): 4–15% B for 5 min, 15-50% B for 50 min, and 50-90% B for 15 min. Mass spectrometry data was acquired using a data dependent acquisition procedure with a cyclic series of a full scan

with resolution of 120,000 followed by MS/MS (HCD, relative collision energy 27%) of the 20 most intense ions and a dynamic exclusion duration of 20 sec.

***Database Search:*** The peak list of the LC-MS/MS were generated by Thermo Proteome Discoverer (v. 2.1) into MASCOT Generic Format (MGF) and searched against the *3D7* database at PlasmoDB and *Pf*ATP4 specific *Dd2* sequences, in addition to a database composed of common lab contaminants using in house version of X!Tandem (48). Search parameters were as follows: fragment mass error: 20 ppm, parent mass error: +/- 7 ppm; fixed modification: carbamidomethylation on cysteine; flexible modifications: Oxidation on Methionine; protease specificity: trypsin (C-terminal R/K unless followed by P), with 1 miss-cut at preliminary search and 5 miss-cut during refinement. Only spectra with log e <-2 were included in the final report.



**Acknowledgments**

We thank Dr. Haiyan Zheng, Dr. David Sleat and Dr. Peter Lobel from Centre for Integrative proteomics at Rutgers University for LC-MS/MS experiments. Dr. Jacquin Niles for the pMG75-ATP4 vector and Dr. David Fidock for the NF54*attB* parasite line. This work was supported by NIH grant R01-AI132508.

**Author Contributions**

A.B.V, L.W.B, A.A.R, M.W.M conceptualized and designed the research. A.A.R, J.M.M, L.W.B, M.W.M performed the research. T.M.D generated the *Pf*ATP4 antibody. A.A.R, M.W.M, J.M.M and A.B.V performed data analysis. A.A.R and A.B.V wrote the manuscript and all authors contributed to editing the manuscript.

**References**

1. F. J. Gamo *et al.*, Thousands of chemical starting points for antimalarial lead identification. *Nature* **465**, 305-310 (2010).
2. W. A. Guiguemde *et al.*, Chemical genetics of Plasmodium falciparum. *Nature* **465**, 311-315 (2010).

3. D. Plouffe *et al.*, In silico activity profiling reveals the mechanism of action of antimalarials discovered in a high-throughput screen. *Proc Natl Acad Sci U S A* **105**, 9059-9064 (2008).
4. J. N. Burrows *et al.*, New developments in anti-malarial target candidate and product profiles. *Malar J* **16**, 26 (2017).
5. M. Rottmann *et al.*, Spiroindolones, a potent compound class for the treatment of malaria. *Science* **329**, 1175-1180 (2010).
6. N. J. White *et al.*, Spiroindolone KAE609 for falciparum and vivax malaria. *The New England journal of medicine* **371**, 403-410 (2014).
7. M. B. Jimenez-Diaz *et al.*, (+)-SJ733, a clinical candidate for malaria that acts through ATP4 to induce rapid host-mediated clearance of Plasmodium. *Proc Natl Acad Sci U S A* **111**, E5455-5462 (2014).
8. A. B. Vaidya *et al.*, Pyrazoleamide compounds are potent antimalarials that target Na+ homeostasis in intraerythrocytic Plasmodium falciparum. *Nature communications* **5**, 5521 (2014).
9. N. J. Spillman *et al.*, Na(+) regulation in the malaria parasite Plasmodium falciparum involves the cation ATPase PfATP4 and is a target of the spiroindolone antimalarials. *Cell Host Microbe* **13**, 227-237 (2013).
10. A. S. M. Dennis, A. M. Lehane, M. C. Ridgway, J. P. Holleran, K. Kirk, Cell Swelling Induced by the Antimalarial KAE609 (Cipargamin) and Other PfATP4-Associated Antimalarials. *Antimicrob Agents Chemother* **62** (2018).
11. S. Das *et al.*, Na+ Influx Induced by New Antimalarials Causes Rapid Alterations in the Cholesterol Content and Morphology of Plasmodium falciparum. *PLoS Pathog* **12**, e1005647 (2016).
12. A. S. M. Dennis, J. E. O. Rosling, A. M. Lehane, K. Kirk, Diverse antimalarials from whole-cell phenotypic screens disrupt malaria parasite ion and volume homeostasis. *Sci Rep* **8**, 8795 (2018).
13. A. M. Lehane, M. C. Ridgway, E. Baker, K. Kirk, Diverse chemotypes disrupt ion homeostasis in the Malaria parasite. *Mol Microbiol* **94**, 327-339 (2014).
14. S. Bhatnagar, S. Nicklas, J. M. Morrisey, D. E. Goldberg, A. B. Vaidya, Diverse Chemical Compounds Target Plasmodium falciparum Plasma Membrane Lipid Homeostasis. *ACS Infect Dis* **5**, 550-558 (2019).
15. G. M. Goldgof *et al.*, Comparative chemical genomics reveal that the spiroindolone antimalarial KAE609 (Cipargamin) is a P-type ATPase inhibitor. *Sci Rep* **6**, 27806 (2016).
16. E. L. Flannery *et al.*, Mutations in the P-type cation-transporter ATPase 4, PfATP4, mediate resistance to both aminopyrazole and spiroindolone antimalarials. *ACS chemical biology* **10**, 413-420 (2015).
17. A. HJ, How do P-Type ATPases transport ions? . *Bioelectrochemistry* **63**, 149-156. (2004).
18. M. G. Palmgren, P. Nissen, P-type ATPases. *Annual review of biophysics* **40**, 243-266 (2011).
19. K. B. Axelsen, M. G. Palmgren, Evolution of substrate specificities in the P-type ATPase superfamily. *J Mol Evol* **46**, 84-101 (1998).
20. C. Toyoshima, T. Mizutani, Crystal structure of the calcium pump with a bound ATP analogue. *Nature* **430**, 529-535 (2004).

21. C. Toyoshima, H. Ogawa, A. Hirata, J. Tsueda, G. Inesi, Crystal structures of the calcium pump and sarcolipin in the Mg2+-bound E1 state. *Nature* **14**, 260-264 (2013).
22. T. L. Sorensen, J. V. Moller, P. Nissen, Phosphoryl transfer and calcium ion occlusion in the calcium pump. *Science* **304**, 1672-1675 (2004).
23. D. L. Stokes, N. M. Green, Structure and function of the calcium pump. *Annu Rev Biophys Biomol Struct* **32**, 445-468 (2003).
24. M. Bublitz, H. Poulsen, J. P. Morth, P. Nissen, In and out of the cation pumps: P-type ATPase structure revisited. *Curr Opin Struct Biol* **20**, 431-439 (2010).
25. J. P. Morth *et al.*, A structural overview of the plasma membrane Na+,K+-ATPase and H+-ATPase ion pumps. *Nat Rev Mol Cell Biol* **12**, 60-70 (2011).
26. J. P. Morth *et al.*, Crystal structure of the sodium-potassium pump. *Nature* **450**, 1043-1049 (2007).
27. W. Kuhlbrandt, Biology, structure and mechanism of P-type ATPases. *Nat Rev Mol Cell Biol* **5**, 282-295 (2004).
28. B. Benito, B. Garciadeblas, P. Schreier, A. Rodriguez-Navarro, Novel p-type ATPases mediate high-affinity potassium or sodium uptake in fungi. *Eukaryot Cell* **3**, 359-368 (2004).
29. A. Rodriguez-Navarro, B. Benito, Sodium or potassium efflux ATPase a fungal, bryophyte, and protozoal ATPase. *Biochim Biophys Acta* **1798**, 1841-1853 (2010).
30. M. A. Reuben, L. S. Lasater, G. Sachs, Characterization of a beta subunit of the gastric H+/K(+)-transporting ATPase. *Proc Natl Acad Sci U S A* **87**, 6767-6771 (1990).
31. S. M. Ganesan, A. Falla, S. J. Goldfless, A. S. Nasamu, J. C. Niles, Synthetic RNA-protein modules integrated with native translation mechanisms to control gene expression in malaria parasites. *Nature communications* **7**, 10727 (2016).
32. L. J. Nkrumah *et al.*, Efficient site-specific integration in Plasmodium falciparum chromosomes mediated by mycobacteriophage Bxb1 integrase. *Nat Methods* **3**, 615-621 (2006).
33. N. Tsunekawa, H. Ogawa, J. Tsueda, T. Akiba, C. Toyoshima, Mechanism of the E2 to E1 transition in Ca(2+) pump revealed by crystal structures of gating residue mutants. *Proc Natl Acad Sci U S A* **115**, 12722-12727 (2018).
34. H. M. Staines, J. C. Ellory, K. Kirk, Perturbation of the pump-leak balance for Na(+) and K(+) in malaria-infected erythrocytes. *Am J Physiol Cell Physiol* **280**, C1576-1587 (2001).
35. C. Toyoshima, R. Kanai, F. Cornelius, First crystal structures of Na+,K+-ATPase: new light on the oldest ion pump. *Structure* **19**, 1732-1738 (2011).
36. C. Toyoshima, M. Nakasako, H. Nomura, H. Ogawa, Crystal structure of the calcium pump of sarcoplasmic reticulum at 2.6 A resolution. *Nature* **405**, 647-655 (2000).
37. C. Toyoshima, Ion pumping by calcium ATPase of sarcoplasmic reticulum. *Adv Exp Med Biol* **592**, 295-303 (2007).
38. C. Toyoshima, Structural aspects of ion pumping by Ca2+-ATPase of sarcoplasmic reticulum. *Arch Biochem Biophys* **476**, 3-11 (2008).

39. C. Toyoshima, G. Inesi, Structural basis of ion pumping by Ca2+-ATPase of the sarcoplasmic reticulum. *Annu Rev Biochem* **73**, 269-292 (2004).
40. D. Gong *et al.*, Structure of the human plasma membrane Ca(2+)-ATPase 1 in complex with its obligatory subunit neuroplastin. *Nature communications* **9**, 3623 (2018).
41. E. Natan, J. N. Wells, S. A. Teichmann, J. A. Marsh, Regulation, evolution and consequences of cotranslational protein complex assembly. *Current opinion in structural biology* **42**, 90-97 (2017).
42. A. Shiber *et al.*, Cotranslational assembly of protein complexes in eukaryotes revealed by ribosome profiling. *Nature* **561**, 268-272 (2018).
43. H. Ke, S. Dass, J. M. Morrisey, M. W. Mather, A. B. Vaidya, The mitochondrial ribosomal protein L13 is critical for the structural and functional integrity of the mitochondrion in Plasmodium falciparum. *The Journal of biological chemistry* **293**, 8128-8137 (2018).
44. A. M. Lehane *et al.*, Characterization of the ATP4 ion pump in Toxoplasma gondii. *J Biol Chem* **294**, 5720-5734 (2019).
45. S. F. Altschul, W. Gish, W. Miller, E. W. Myers, D. J. Lipman, Basic local alignment search tool. *Journal of molecular biology* **215**, 403-410 (1990).
46. N. R. Coordinators, Database resources of the National Center for Biotechnology Information. *Nucleic acids research* **44**, D7-D19 (2016).
47. C. Aurrecoechea *et al.*, EuPathDB: the eukaryotic pathogen genomics database resource. *Nucleic acids research* **45**, D581-D591 (2017).
48. R. Craig, J. P. Cortens, R. C. Beavis, Open source system for analyzing, validating, and storing protein identification data. *Journal of proteome research* **3**, 1234-1242 (2004).
49. A. R. Mól, M. S. Castro, W. Fontes, NetWheels: A web application to create high quality peptide helical wheel and net projections. *bioRxiv* 10.1101/416347, 416347 (2018).
50. S. Bienert *et al.*, The SWISS-MODEL Repository-new features and functionality. *Nucleic acids research* **45**, D313-D319 (2017).

# Figures

Figure 1

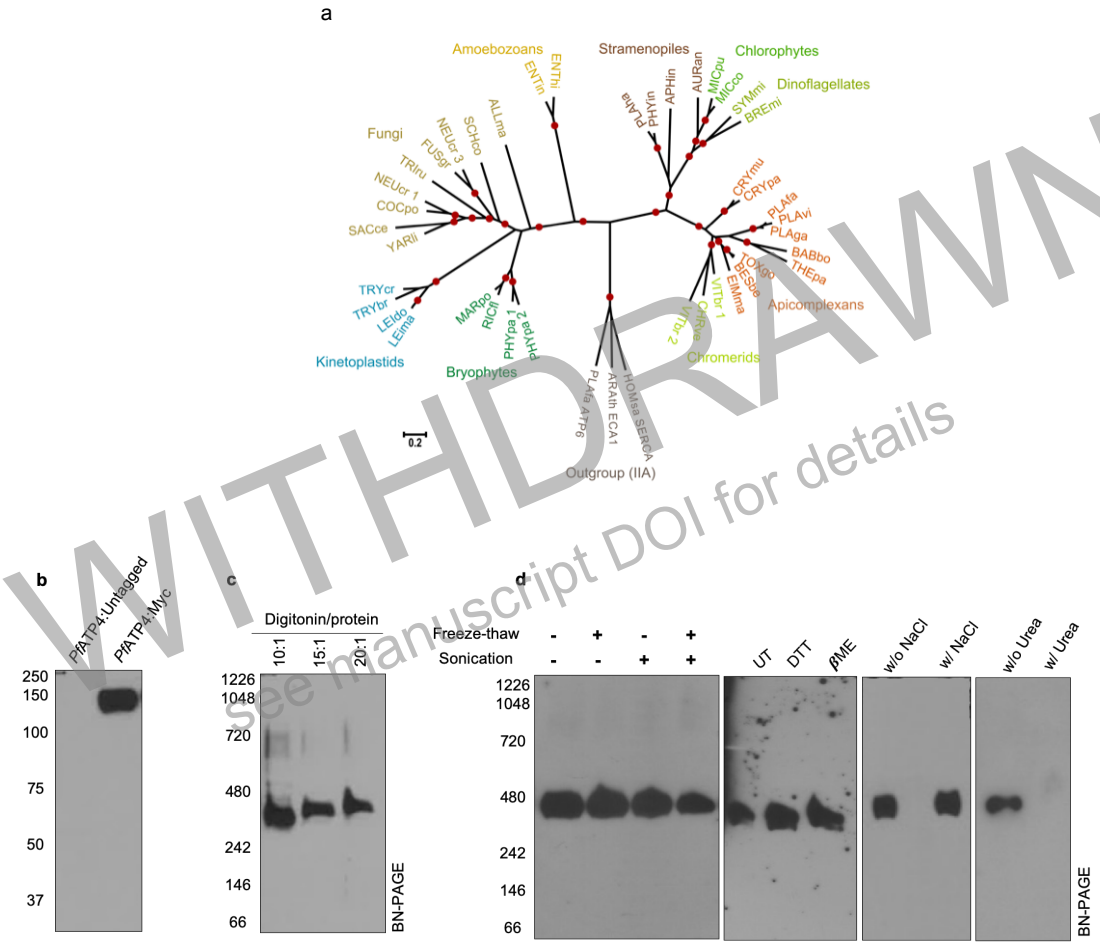


**Figure 1. *Pf*ATP4 forms a distinct group among PIID type ATPases and is present as a large complex in its native state.** a) Phylogenetic analysis of PIID ATPases, depicted as a radial tree diagram with PIIA ATPases as outgroups; Red dots indicate >90% boot strap support. See *SI Appendix, Table S1* for full list and abbreviations. *b*) Western blots after SDS-PAGE (Panel 1) of membrane preparations from untagged and *NF54attBPf*ATP4:Myc parasites probed with anti-c-Myc depicting a 140kd band corresponding to *Pf*ATP4. c) Western blots of *NF54attBPf*ATP4:Myc parasites analyzed on a BN-PAGE after overnight solubilization with indicated ratios of digitonin:protein displaying a band at a higher molecular weight (between 242-480kd). d) Digitonin solubilized samples from *NF54attBPf*ATP4:Myc parasites were subjected to freeze thawing (3x) and/or sonication (2x10 min) before overnight solubilization with 2% digitonin (Panel 1); a 30min treatment with 10 mM DTT or 20 mM ßME after solubilization (Panel 2); solubilization in the presence or absence of 200mM NaCl (Panel 3) or 8M urea (panel 4). The Western blots were probed with anti-c-Myc.

Figure 2

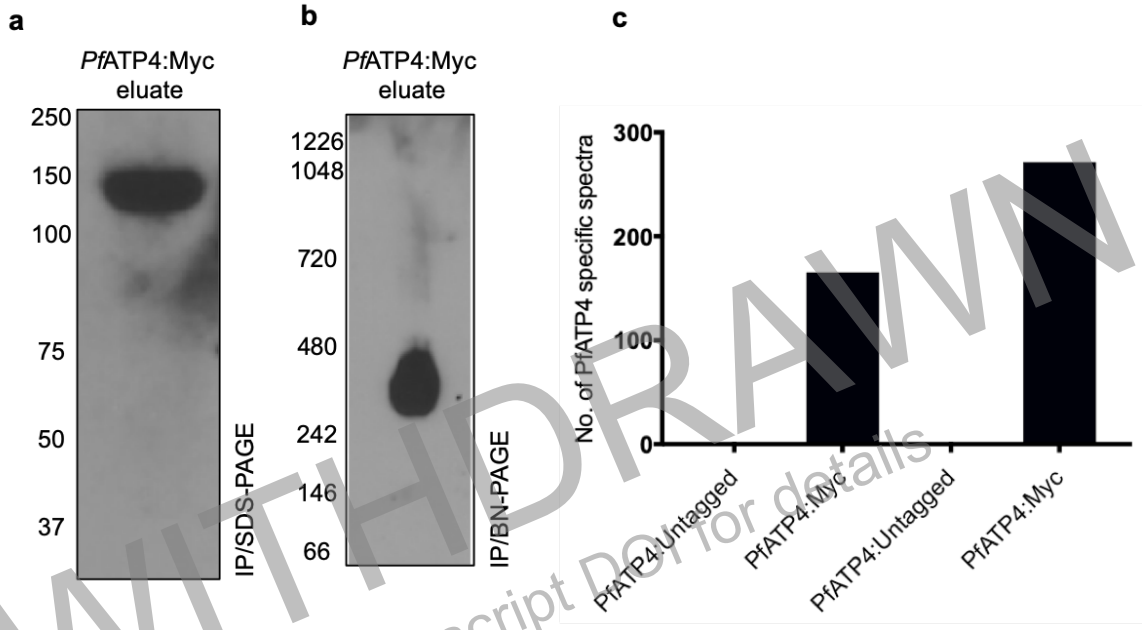




**Figure 2. *Pf*ATP4 complex is homooligomeric in nature.** Western blot detection after immunopulldown (IP) of *Pf*ATP4 probed with anti-cMyc after the eluate was run on an a) SDS-PAGE and b) BN-PAGE gel indicating that *Pf*ATP4 remains as a complex after pulldown. c) Proteomic analysis showing counts of peptide spectra originating from *Pf*ATP4 in two biological replicates of immunopulldowns from untagged and c-Myc tagged parasites. Peptides common to both samples were considered as non-specific contaminants during pulldown and were eliminated during analysis. Except for PfATP4 no other proteins were represented uniquely in c-Myc-tagged pulldowns.

Figure 3

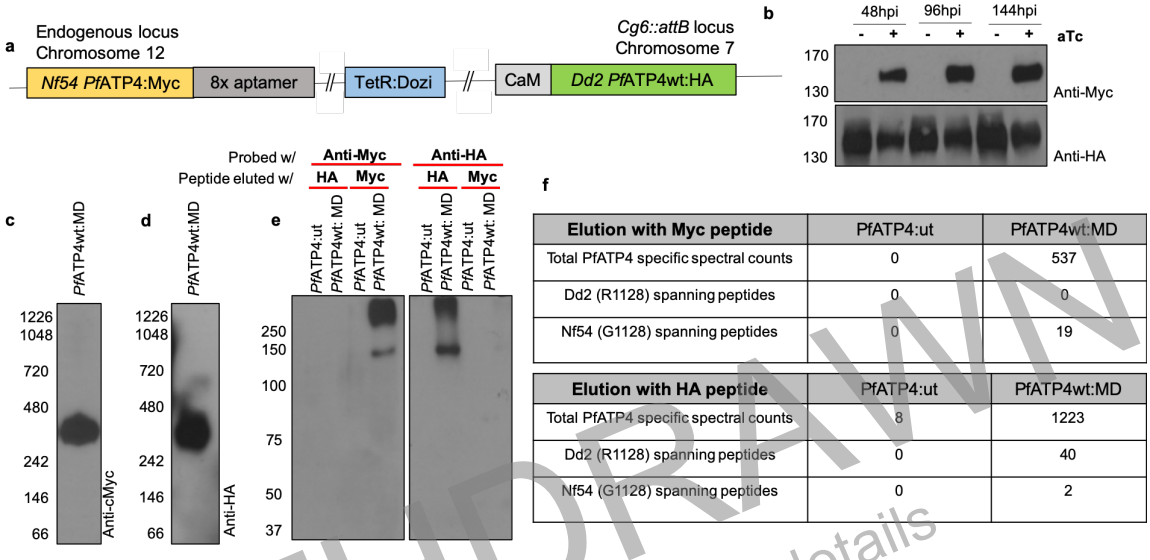


f

| Elution with Myc peptide | PfATP4:ut | PfATP4wt:MD |
|---|---|---|
| Total PfATP4 specific spectral counts | 0 | 537 |
| Dd2 (R1128) spanning peptides | 0 | 0 |
| Nf54 (G1128) spanning peptides | 0 | 19 |

| Elution with HA peptide | PfATP4:ut | PfATP4wt:MD |
|---|---|---|
| Total PfATP4 specific spectral counts | 8 | 1223 |
| Dd2 (R1128) spanning peptides | 0 | 40 |
| Nf54 (G1128) spanning peptides | 0 | 2 |



**Figure 3: Assembly of *Pf*ATP4 into a complex is co-translational.** a) Schematic representation of the merodiploid (MD) parasite line expressing aTc regulated *Nf54Pf*ATP4:Myc at the endogenous locus, and *Dd2 Pf*ATP4:3HA at the *cg6::attB* locus expressed under the control of the calmodulin promoter. b) SDS-PAGE followed by western blotting of merodiploid *Nf54Pf*ATP4:Myc*attB Pf*ATP4:wtHA parasite lysate maintained with and without aTc over 48, 96 and 144 hours post invasion (hpi) probed with anti-c-Myc and anti-HA to detect the expression of *Pf*ATP4 from the endogenous (top) and ectopic loci (bottom) indicating that the ectopic expression of *Pf*ATP4 remains stable upon knockdown of the endogenous *Pf*ATP4 c) Endogenous and d) ectopic *Pf*ATP4 expression from the merodiploid *Nf54Pf*ATP4:Myc*attBPf*ATP4:wtHA parasite on a BN-gel, followed by western blotting with anti-c-Myc and anti-HA showing co-dominant complex formation. e) Western blot and f) Proteomic analysis after immunopulldown (IP) of untagged (*Pf*ATP4:ut) and merodiploid (*Pf*ATP4:wtMD) parasites showing the presence of only cognate peptide spectra spanning the polymorphic region.

Figure 4

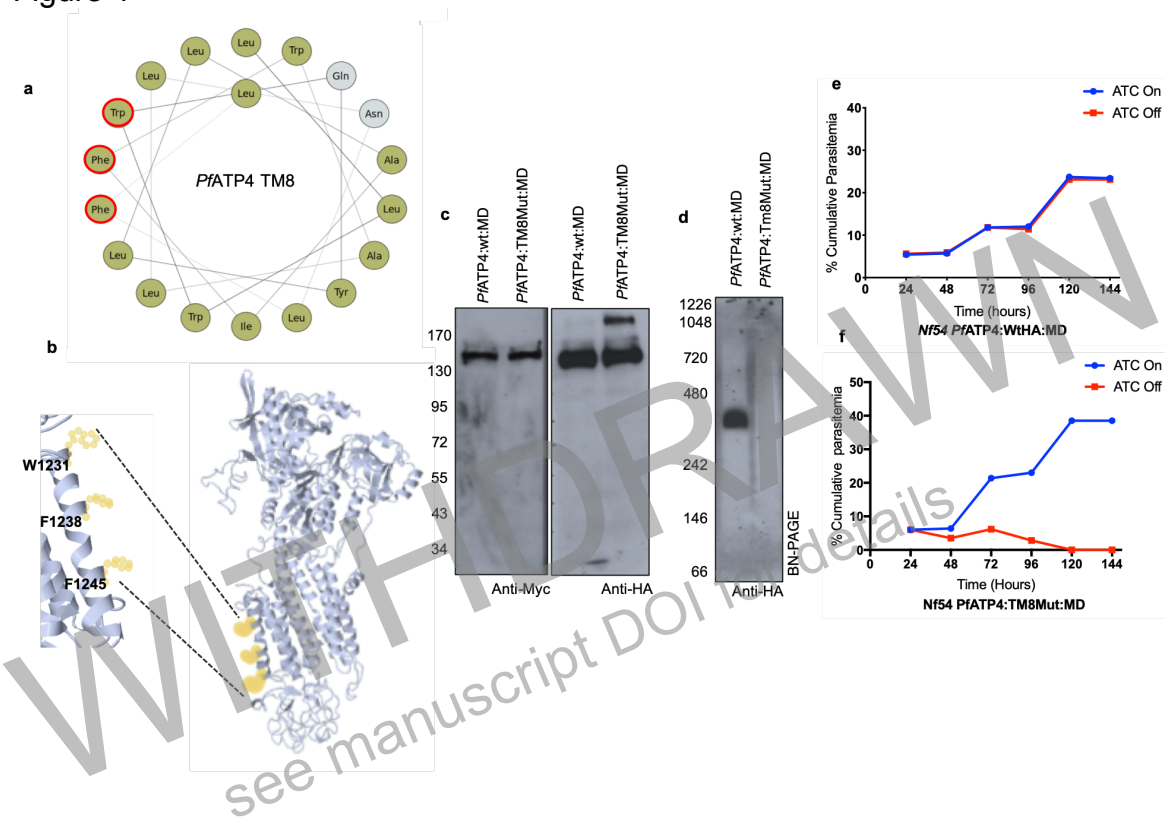




**Figure 4: Transmembrane helix 8 is involved in *Pf*ATP4 oligomerization.** (a) Helical wheel projection of *Pf*ATP4 TM8 helix, generated by NetWheels program(49). (b) monomeric *PfATP4* model generated by using SWISS-MODEL (50)highlighting the aromatic amino acids (W1231, F1238, F1245) in TM8 stacking vertically along a surface of the protein. (c) SDS- PAGE followed by western blot of lysates from Nf54*Pf*ATP4Myc*attBPf*ATP4:wtHA (*Pf*ATP4:wtMD) and Nf54*Pf*ATP4Myc*attBPf*ATP4:TM8Mut (*Pf*ATP4:Tm8MutMD) merodiploid parasites to detect endogenous (probed with anti-c-myc) and ectopic PfATP4 expression (probed with anti-HA). (d) BN-gel analysis of ectopic *Pf*ATP4 expression (e,f) Growth curves as estimated by cumulative parasitemia of wildtype and mutant merodiploid lines with and without aTc (e,f) Representative growth curves (of 3 biological replicates) *Pf*ATP4:wtMD (e) and *Pf*ATP:Tm8MutMD (f) parasite lines grown in the presence or absence of 250 nM aTc. Cultures were split 1:2 at 48 and 96hpi. Parasitemia was determined by counting at least 1000 red blood cells in each Giemsa-stained thin blood smear. Cumulative parasitemia was determined by multiplication of parasitemia and split factor (in this case, 2) over the time course.